THE UNIVERSITY OF
WARWICK

University of Warwick institutional repository: http://go.warwick.ac.uk/wrap

This paper is made available online in accordance with
publisher policies. Please scroll down to view the document
itself. Please refer to the repository record for this item and our
policy information available from the repository home page for
further information.

To see the final version of this paper please visit the publisher's website.
Access to the published version may require a subscription.

Author(s): Barbara Pierscionek, Roger J. Green, and Sergey G. Dolgobrodov
Article Title: Intraocular Light Scatter as Modeled Through a Stratified Medium
Year of publication: 2001
Link to published article:
http://dx.doi.org/10.1364/AO.40.006340
Publisher statement: Pierscionek, B., Green, R. J. and Dolgobrodov, S. G. (2001). Intraocular Light Scatter as Modeled Through a Stratified Medium. Applied Optics, 40(34), pp. 6340-6348. © 2001 The Optical Society. This paper was published in Applied Optics and is made available as an electronic reprint with the permission of OSA. The paper can be found at the following URL on the OSA website: http://dx.doi.org/10.1364/AO.40.006340. Systematic or multiple reproduction or distribution to multiple locations via electronic or other means is prohibited and is subject to penalties under law.

Intraocular light scatter as modeled through a stratified medium

Barbara Pierscionek, Roger J. Green, and Sergey G. Dolgobrodov

Intraocular light scatter is modeled through a stratified medium. It is shown that the eye lens possesses properties of an interference filter. In conditions that may mimic opacification, as found with cataract formation, such a filter may have stop zones with reflectance up to 1 in the band of visible light.
© 2001 Optical Society of America
OCIS codes: 170.4470, 170.4730, 330.5020, 330.3790, 310.6860, 290.1350.

1. Introduction

The mode of growth of the eye lens is such that, although accretion continues on the surface, inner cells are never shed. Hence, with age, structural degradation takes place and this can lead to impedance of light transmission in the older eye. When this progresses to a level of opacification, which causes visual impairment, it is termed senile cataract and is one of the major causes of low vision in the elderly.

The classical theory of Benedek[1,2] attempts to explain that the cause of opacification in cataract is the result of local, pointwise refractive-index fluctuations that cause light to scatter. However, the theory is insufficient to explain all the phenomena observed in experiments. In particular it assumes that the lens proteins are spheres of uniform index; it does not take into account the fact that the refractive index in the human lens is nonhomogeneous but increases from periphery to center.[3,4] More importantly, it considers light scatter only in the cataractous process, i.e., when the scatter is at an advanced stage. Furthermore, Benedek's theory considers protein aggregation as the main mechanism for cataract formation. Such an important morphological property as stratification is not mentioned.

An accurate model of light transmission through the lens needs to take into account all the relevant lenticular optical parameters: its physical dimensions (shape or curvature) and the refractive-index gradient, as well as the contribution of scatter and absorption that occur to differing proportions in the various types of cataract. The main causes of light-scattering turbidity in the eye lens are fluctuations in the refractive index over spatial domains, comparable to the wavelength of the light. The structural organization of the lens, however, may play an important role in any scattering effects.

The eye lens is composed of onionlike layers of fiber cells that stretch from anterior to posterior poles (the poles lie on the optic axis). This particular morphology results in Weiner body-type layering (plates shaped as rhomboids) in which the cells have a different refractive index from that found in the boundary regions (gaps) containing cell membranes and extracellular fluid.[5–7] These conditions will produce the interference phenomenon for light going through a stratified structure. Moreover, such a multiplicity of thin-film structures can operate as interference filters with an impedance reaching a maximum value of 1.[8–11]

Our main aim in this research is to estimate the amount of light that is forward scattered and backscattered by the cell (cytoplasmic) layers and gaps between the cells packed within the lens in a regular stratified structure (see Fig. 1). The transparent eye lens represents heterogeneous media (composed mainly of random structures) with smooth space variations in refractive and absorption indices. The formation of an opacity, manifested as cataract, results from a rise in the periodical discontinuity of refractive-index values on the surfaces between lens fibers.[5,7,12] It is assumed that the refractive-index fluctuations and anisotropy in turn result from space

B. Pierscionek is with the Department of Biomedical Sciences, University of Bradford, Bradford BD7 1DP, UK. R. J. Green and S. G. Dolgobrodov (essqh@warwick.ac.uk) are with the School of Engineering, University of Warwick, Coventry CV4 7AL, UK.

Received 10 August 2000; revised manuscript received 10 July 2001.

0003-6935/01/346340-09$15.00/0
© 2001 Optical Society of America

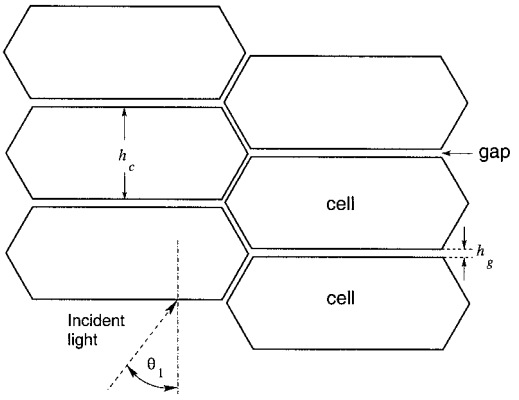

Fig. 1. Morphological structure of the crystalline lens, as on a normal cut. Thickness of the rhomboidal fibers: $h_c \approx 8$ μm, widths of the boundary regions h_g from 20 nm up to 700 nm.

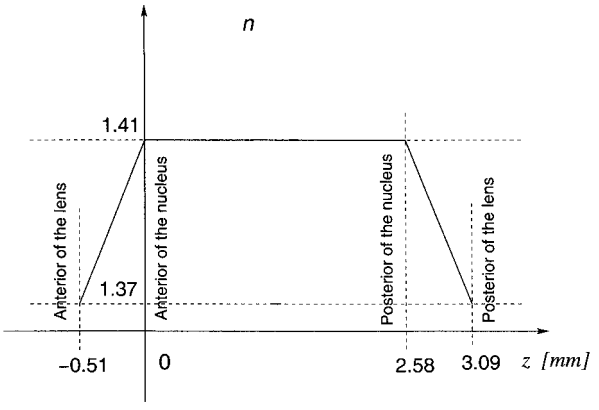

Fig. 2. Refractive index in the normal eye: up to ≈1.4 in the center of the nucleus and a linear variation in the outer region of the nucleus from ≈1.37 at the cortex.[5] The origin of frame references coincides with the anterior of the area with a higher refractive index. Axis 0, z coincides with the visual axis of the lens.

fluctuations in the widths of the lens fibers and of the narrow boundary regions between fibers. In this context it is worth noting the age-related changes in lens water regulations[13] and that, with cataract, lens cells may swell.[14] For example, it was calculated that a 14% swelling of the lens caused by influx water may increase the turbidity by 20–40%.[5] Both factors will impact on the dimensions (widths and shape) of the fiber cells and boundary regions. The contribution of these changes in structure to scattering and reflection is of particular interest. A similar approach was discussed previously by Hemenger.[7]

2. Methods

A. Common Case

We denote a position vector of a typical point on a ray by $\mathbf{r}$ and the length of the ray (natural parameter of the curve) from a fixed point on it by s. The tangent vector $\mathbf{s} = \mathrm{d}\mathbf{r}/\mathrm{d}s$. According to conditions for a gradient-index structure, the refractive index n is a function of the space coordinate: $n = n(\mathbf{r})$. The basic optical equation is the eikonal equation for the eikonal function $\mathcal{J}(\mathbf{r})$[11]:

$$(\nabla \mathcal{J})^2 = n^2(\mathbf{r}). \tag{1}$$

The geometric wave fronts are the level surfaces $\mathcal{J}(\mathbf{r}) = \text{const}$. It follows from Eq. (1) that the ray trace must satisfy the following differential equation[11]:

$$\frac{\mathrm{d}}{\mathrm{d}s}\left(n\,\frac{\mathrm{d}\mathbf{r}}{\mathrm{d}s}\right) = \operatorname{grad} n. \tag{2}$$

Given

$$\mathbf{r}_0 = \mathbf{r}(s_0), \tag{3}$$

$$\mathbf{s}_0 = \mathbf{s}(s_0), \tag{4}$$

the Cauchy problem for Eq. (2) can be solved for any particular n.[15]

For homogeneous media and constant n, we have $\mathrm{d}^2\mathbf{r}/\mathrm{d}s^2 = 0$ and $\mathbf{r} = \mathbf{a}s + \mathbf{b}$ ($\mathbf{a}$ and $\mathbf{b}$ are constant vectors). The latter is the vector equation of a straight line in the direction of vector $\mathbf{a}$, passing through the point $\mathbf{r} = \mathbf{b}$, and corresponds to classical ray tracing.[16]

B. Paraxial Approximation

We restrict ourselves to the paraxial (Gaussian) approximation when all the rays involved are confined to a region enclosing the optical axis and having infinitesimal dimensions perpendicular to it.[11] Consequently all angles involved are of infinitesimal size and (a) any paraxial angle is equal to its sine or tangent and (b) the cosine or secant of any paraxial angle is equal to unity.

For heterogeneous, stratified media with Cartesian coordinates (x, y, z), let us suppose that n is a linear function depending only on the coordinate z, $n(\mathbf{r}) = \alpha z + n_0$, $z \geq 0$, and $n = n_0$ for $z < 0$. This case is of considerable importance in paraxially approximated ray tracing through the eye lens, in which the pattern of refractive-index variation is as shown in Fig. 2. This can be rewritten as projections on the coordinate axes:

$$n\,\frac{\mathrm{d}^2x}{\mathrm{d}s^2} = 0, \tag{5}$$

$$n\,\frac{\mathrm{d}^2y}{\mathrm{d}s^2} = 0, \tag{6}$$

$$n\,\frac{\mathrm{d}^2z}{\mathrm{d}s^2} + \frac{\mathrm{d}n}{\mathrm{d}s}\,\frac{\mathrm{d}z}{\mathrm{d}s} = \frac{\partial n}{\partial z} = \alpha. \tag{7}$$

Because $n \neq 0$, one obtains

$$x = a_x s + b_x, \tag{8}$$

$$y = a_y s + b_y, \tag{9}$$

where a_x, b_x, a_y, b_y are constants.

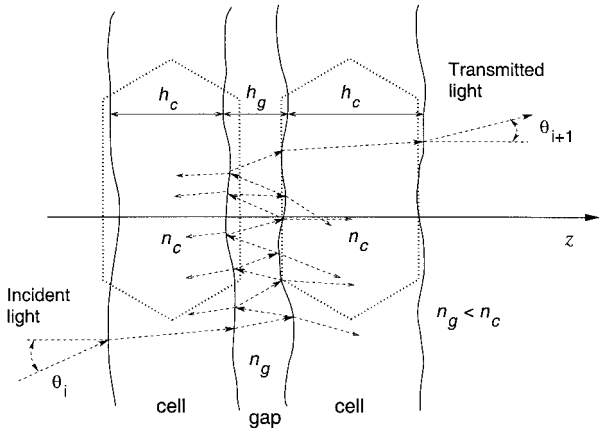

Fig. 3. Displacement of a multiply reflected ray along the thin fluid-filled regions between two cellular layers with irregular surfaces and of greater refractive index. Two rhomboid fibers are shown schematically by dotted lines.

Because $dn/ds = (d\mathbf{r}/ds \cdot \nabla)\, n = \alpha\, dz/ds$, Eq. (7) can be rewritten as

$$\left(z + \frac{n_0}{\alpha}\right)\frac{d^2z}{ds^2} + \left(\frac{dz}{ds}\right)^2 = 1. \tag{10}$$

The solutions of Eq. (10) satisfying the initial conditions

$$z(0) = z_0, \tag{11}$$

$$z'(0) = z_0', \tag{12}$$

where z_0 and z_0' are constants, are

$$z_{1,2}(s) = \frac{1}{\alpha}\{-n_0 \pm [n_0^2 + 2s\alpha z_0'(\alpha z_0 + n_0) + \alpha z_0(\alpha z_0 + 2n_0) + \alpha^2 s^2]^{1/2}\}. \tag{13}$$

In the intact human lens the spatial distributions of the refractive index vary along the optic axis reaching a value of 1.41 in the center of the nucleus, with approximately linear variations in the cortex starting from ≈1.37 at the extreme periphery.[4,5] A model of the gradient of refractive index is shown in Fig. 2.

C. Analysis of Stratified Media

When monochromatic, plane-polarized light waves pass through a thin-layer combination of cellular fibers and liquidlike boundary regions, the zigzag reflections give rise, in the most general case, to two resultant trains of waves advancing in opposite directions (see Fig. 3). These will interfere and lead to a complex picture of the resultant electric and magnetic fields.

In *in vitro* experiments, the forward-scattered and backscattered light can be investigated independently of any transmission alterations through the cornea,[12,17] and our model mimics this situation. In this study, we consider only the central or nuclear part of the lens where the refractive index of the cellular fibers is highest and most constant in value. It is also the region that contains the oldest cells in the lens and hence is the most prone to the age-related changes, some of which may be cataractous.

For the purpose of modeling, we simplify the real morphological picture (see Fig. 1) and suppose that fiber cells are continuous in a plane that is orthogonal to the light incidence and that they form a simple, regular, stratified structure. Moreover, we neglect any absorption inside the medium. In a normal (noncataractous) lens, absorption does not affect ray passage significantly. Two rhomboid fibers are shown schematically by dotted lines in Fig. 3. Scattering becomes pronounced when the boundary region width is comparable to the wavelength, as is probable in the case of morphological degradation that may eventually lead to cataract.[2,14,18] It should be noted that fiber cells may also thicken with age because of adhesion of protein.[19] This is supported by recent findings showing that the stiffening or loss of elasticity in the lens with age is due to a change in the fiber cell membranes,[20] and this rigidity is most likely to occur because of thickening. Such a stratified structure will possess birefringence; to minimize the light scattering, which is inevitable from birefringence of form, some supramolecular organization within the fiber cells must provide intrinsic birefringence to minimize the optical anisotropy. In this study we estimate the scattering and dispersion in such a stratified structure.

It is sufficient to consider only the case of the linearly polarized electric wave with its electric vector perpendicular to the plane of incidence [transverse-electric (TE) wave]. Any arbitrary polarized plane wave can be resolved into two waves: TE wave and the TM (transverse-magnetic) wave.[11] Because the boundary conditions at the borders of layers are independent of each other, these two waves will also be mutually independent. In addition, because Maxwell's equations remain unchanged when the electric field vector **E** and the magnetic field vector **H** and simultaneously the dielectric permeability and magnetic permeability are interchanged, all further discussions of TE waves are applicable to TM waves.[11]

In the case of a stratified medium with a constant dielectric and magnetic permeability ϵ and μ, and hence constant refractive index $n = \sqrt{\epsilon\mu}$, Maxwell's equations for amplitudes of the electrical U and magnetic V components of a monochromatic TE wave with wavelength λ_0 reduce to the following scalar equations:

$$\frac{d^2U}{dz^2} + (k_0^2 n^2 \cos^2\theta)U = 0, \tag{14}$$

$$\frac{d^2V}{dz^2} + (k_0^2 n^2 \cos^2\theta)V = 0, \tag{15}$$

where θ denotes the angle that the normal to the wave makes with the z axis and $k_0 = 2\pi/\lambda_0$ is the wave number.

According to Abelès[21] the propagation of a plane monochromatic electromagnetic wave through strat-

ified homogeneous nonabsorbing media with axis 0, z is completely determined by its characteristic matrix[22,23]:

$$M(z) = \begin{bmatrix} \cos(k_0 n z \cos\theta) & -\frac{i}{p}\sin(k_0 n z \cos\theta) \\ -ip\sin(k_0 n z \cos\theta) & \cos(k_0 n z \cos\theta) \end{bmatrix}, \tag{16}$$

where $p = \sqrt{\epsilon/\mu}\cos\theta$. The matrix $M(z)$ is clearly unimodular and it relates the x and y components of the electric (or magnetic) vectors in the plane $z = 0$ to the components in an arbitrary plane $z = \text{const}$:

$$\begin{pmatrix} U_0 \\ V_0 \end{pmatrix} = M(z)\begin{bmatrix} U(z) \\ V(z) \end{bmatrix}.$$

In the case of a stratified medium that consists of a number N of thin homogeneous layers, the resulting characteristic matrix of the pile is a product of the characteristic matrices:

$$M(z_N) = M_1(z_1)M_2(z_2 - z_1)\ldots M_N(z_N - z_{N-1}), \tag{17}$$

where z_i are the boundary points of the different layers of the pile. The value $\beta = k_0 n(z_N - z_{N-1}) = n\omega(z_N - z_{N-1})/c = 2\pi n(z_N - z_{N-1})/\lambda_0$ is the optical thickness of the Nth layer, measured in units of phase. The above matrix approximation does not account for reflections from the interior of the layer but takes into account the waves reflected from the discontinuities at the boundaries. The variation of the refractive index in the layers solely influences the value of the optical thickness β.

The eye lens is a multilamellar structure, which we consider to consist of a succession of homogeneous layers of alternately high fiber cell interiors and low boundary or gap regions (filled with fluid) with refractive indices n_c and n_g and geometric thicknesses h_c and h_g, respectively. Also, we assume the medium to be nonmagnetic ($\mu = 1$), absolutely conducting, and nonabsorbing.

For the effective optical thicknesses of the layers,

$$\beta_c = \frac{2\pi}{\lambda_0} n_c h_c \cos\theta_c, \tag{18}$$

$$\beta_g = \frac{2\pi}{\lambda_0} n_g h_g \cos\theta_g, \tag{19}$$

and for the optical admittance (load),

$$p_c = n_c \cos\theta_c, \tag{20}$$

$$p_g = n_g \cos\theta_g. \tag{21}$$

If $h = h_c + h_g$, then the characteristic matrix $M_2(h)$ of one period is

$$M_2(h) = \begin{bmatrix} \cos\beta_c\cos\beta_g - \frac{p_g}{p_c}\sin\beta_c\sin\beta_g & -\frac{i}{p_g}\cos\beta_c\sin\beta_g - \frac{i}{p_c}\sin\beta_c\cos\beta_g \\ -ip_c\sin\beta_c\cos\beta_g - ip_g\cos\beta_c\sin\beta_g & \cos\beta_c\cos\beta_g - \frac{p_c}{p_g}\sin\beta_c\sin\beta_g \end{bmatrix}. \tag{22}$$

For N periods we obtain[11,24]

$$M_{2N}(Nh) = \begin{bmatrix} m_{11} & m_{12} \\ m_{21} & m_{22} \end{bmatrix}, \tag{23}$$

where

$$m_{11} = \left(\cos\beta_c\cos\beta_g - \frac{p_g}{p_c}\sin\beta_c\sin\beta_g\right)\mathcal{U}_{N-1}(a) - \mathcal{U}_{N-2}(a), \tag{24}$$

$$m_{12} = -i\left(\frac{1}{p_g}\cos\beta_c\sin\beta_g + \frac{1}{p_c}\sin\beta_c\cos\beta_g\right)\mathcal{U}_{N-1}(a), \tag{25}$$

$$m_{21} = -i(p_c\sin\beta_c\cos\beta_g + p_g\cos\beta_c\sin\beta_g)\mathcal{U}_{N-1}(a), \tag{26}$$

$$m_{22} = \left(\cos\beta_c\cos\beta_g - \frac{p_c}{p_g}\sin\beta_c\sin\beta_g\right)\mathcal{U}_{N-1}(a) - \mathcal{U}_{N-2}(a), \tag{27}$$

$$a = \cos\beta_c\cos\beta_g - \frac{1}{2}\left(\frac{p_c}{p_g} + \frac{p_g}{p_c}\right)\sin\beta_c\sin\beta_g, \tag{28}$$

where $\mathcal{U}_N$ are Chebyshov polynomials of the second kind.[25] We assume the last layer to be a fiber cell with parameters h_c, n_c, and a characteristic matrix

$$M_{2N+1}[(N+1)h] = \begin{bmatrix} \cos\beta_c & -\frac{i}{p_c}\sin\beta_c \\ -ip_c\sin\beta_c & \cos\beta_c \end{bmatrix}. \tag{29}$$

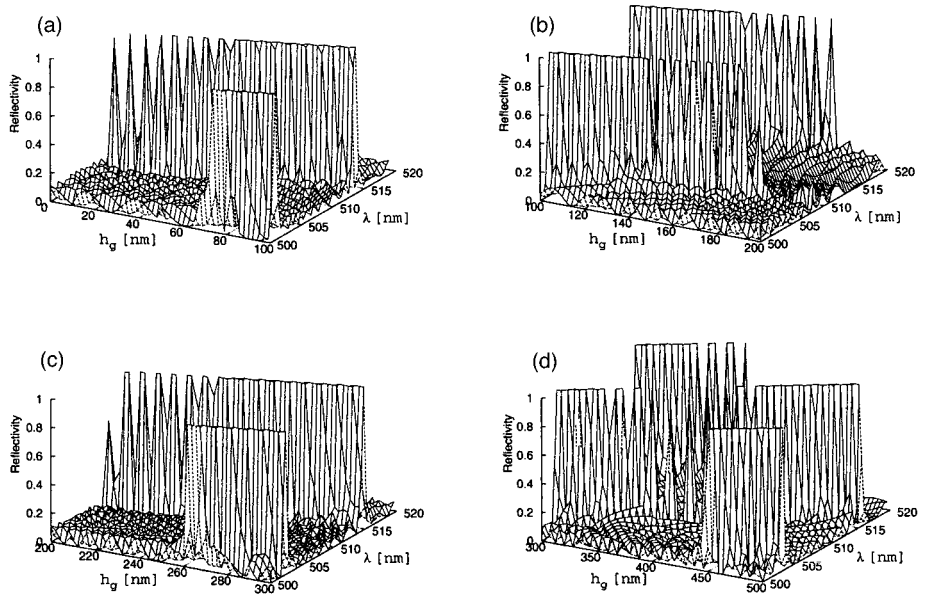

Fig. 4. Dependence of the reflectivity $\mathcal{R}$ for the normal incidence ($\theta_1 = 0°$), $\lambda = 500$–520 nm, $h_c = 7$ μm. (a) $h_g = 0$–100 nm, (b) $h_g = 100$–200 nm, (c) $h_g = 200$–300 nm, (d) $h_g = 300$–500 nm. Parameters correspond to $N \approx 150$–175.

So the characteristic matrix for the nucleus of lens $\mathcal{M}$ is

$$\mathcal{M} = M_{2N} M_{2N+1}. \tag{30}$$

Following conventional notations,[10,11,24] we introduce the amplitude reflection coefficient r as the ratio of amplitude of the electric components of the reflected wave R to that of incident one A:

$$r = \frac{R}{A} = \frac{(\mathcal{M}_{11} + \mathcal{M}_{12} p_g) p_c - \mathcal{M}_{21} + \mathcal{M}_{22} p_g}{(\mathcal{M}_{11} + \mathcal{M}_{12} p_g) p_c + \mathcal{M}_{21} + \mathcal{M}_{22} p_g}, \tag{31}$$

and the notion of reflectivity $\mathcal{R}$:

$$\mathcal{R} = |r|^2. \tag{32}$$

The latter represents the ratio of energy in the reflected ray to the energy in the incident ray. The transmissivity $\mathcal{T}$ of media in the case of normal incidence and when $n_{N+1} = n_1$ is related to reflectivity $\mathcal{R}$ by the law of conservation of energy:

$$\mathcal{R} + \mathcal{T} = 1. \tag{33}$$

For the purpose of evaluation we use measured values of thicknesses for fiber cell and boundary regions, reported in electron microscopic[26] and laser diffraction experiments.[5] The thickness of cellular fibers was estimated to be $h_c \approx 2$–7 μm, and the width of rhomboidal cells was found to be 8–10 μm. The boundary regions are several degrees of magnitude thinner than the cells.[6,7] We assume then that thickness h_g varies approximately between 20 and 700 nm. Therefore the optical thicknesses of these two regions may differ by several orders of magnitude. Also, as mentioned above, we are considering the light transmissivity through the nucleus of the lens, i.e., the region with the highest refractive index of the cell layers (see Fig. 2). In the young lens the d thickness changes with accommodation. The value taken is for the older adult lens, which is no longer able to alter its focus and for which d is therefore fixed. Hence we estimate the thickness of the nucleus to be $d \approx 2.6$ mm.[3,27]

3. Results and Discussion

A. Reflectivity and Polarization Properties

The results of numerical modeling of $\mathcal{R}$ can be seen in Figs. 4–9. For all figures we assume $n_c = 1.41$ and $n_g = 1.33$.

Figure 4 shows $\mathcal{R}$ as a function of light wavelengths λ in the range 500–520 nm for normal incidence $\theta_1 = 0°$ and $h_c = 7$ μm. Boundary region width was taken as $h_g = 0$–100 nm, $h_g = 100$–200 nm, $h_g = 200$–300 nm, and $h_g = 300$–500 nm. In this case $N \approx 150$. It can be seen from Fig. 4(a) that the reflectance tends to zero when h_g tends to zero. This case is similar to that of normal tissue with densely packed fiber cells. The background level of reflectance is less on average than 0.05, which is in concordance with known experimental results.[17] Also it can be noticed from Fig. 4 that the reflectivity has a two-dimensional periodical pattern. The periodic variation is a function of the parameters of the problem. The periodicity of λ can be seen more clearly in Fig. 5, which represents a slice through Fig. 4(b) at $h_g = 120$ nm. The wavelength λ_s of the stop zones (higher reflectance bands) can be easily calculated by the equation[28]

$$\lambda_s = \frac{2}{m} (n_c h_c + n_g h_g), \quad m = 1, 2, \ldots. \tag{34}$$

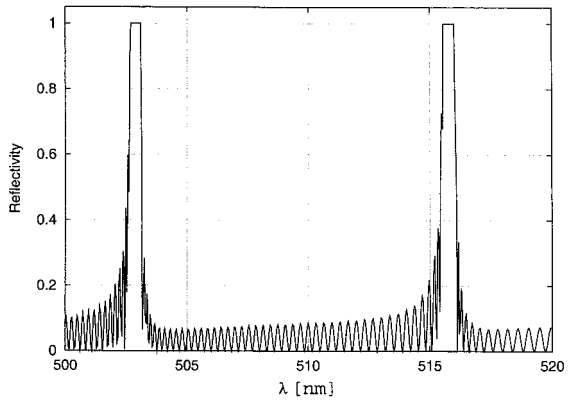

Fig. 5. Slice through Fig. 4(b). Reflectivity $\mathcal{R}$ versus $\lambda = 500$–520 nm; $\theta_1 = 0°$; thickness of layers, $h_c = 7$ μm, $h_g = 120$ nm.

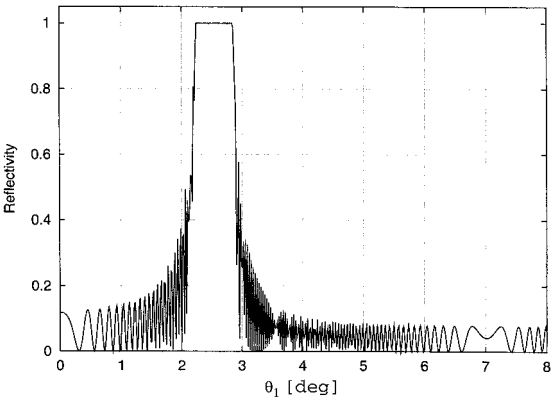

Fig. 7. Slice through Fig. 6. Reflectivity $\mathcal{R}$ versus $\theta_1 = 0°$–8°; thickness of layers, $h_c = 7$ μm, $h_g = 280$ nm; $\lambda = 500$ nm.

The two zones shown in Fig. 5 correspond to $m = 39$, 40.

Figure 6 shows the angular dependence of reflectivity $\mathcal{R}$ for a range of $\theta_1 = 0°$–8°, $h_g = 100$–300 nm, $h_c = 7$ μm, and $\lambda = 500$ nm. Figure 7 shows the slice through Fig. 6 for a fixed value of $h_g = 280$ nm. It can be seen that with these parameters the width of the stop zones is approximately 1° and the period through θ_1 is approximately 10°.

The reflectivity $\mathcal{R}$ dependence on layer thickness is shown in Fig. 8 for $h_c = 7$–8 μm. The range of boundary region widths are given as $h_g = 120$–200 nm and $h_g = 200$–280 nm. Incidence is normal and $\lambda = 500$ nm. Two distinct periods of reflectivity (short and long) along the h_g axis can be seen. Equation (34) can be used to estimate the periodicity in this spatial pattern for a fixed wavelength λ. Equation (34) provides low transmittance bands for $m = 1$, 2, . . . , except when $m = k(a + b)$ $k = 1, 2, \ldots$, where a and b are the smallest possible integers defined by the ratio of the optical thickness[29] $(n_c h_c / n_g h_g) = a/b$. In Fig. 8 it corresponds to the area $h_c \approx 7090$ nm and $h_g \approx 185$ nm (and hence $a/b = 40$, $m = 41$, $k = 1$) where transmittance reaches a maximum.

Figures 4–8 indicate that such a stratified pile structure possesses the properties of an optical interference filter.[9,10,24] The stop zones represent regions in the spectrum where the reflectance of the medium increases and tends to 1. It should be noted that, in the case of the eye lens, these zones are in a visible part of the light spectrum. The zones of discontinuity seen in a live human lens when examined biomicroscopically may represent a region where the stop zones have become thicker, possibly from localized cellular compaction. With age and the accompanying biochemical changes in the protein, further thickening of the stop zones may be a continuing factor in cataract formation.

Figure 9 gives the reflectivity $\mathcal{R}$ dependence on the incident light wavelength (for wavelength $\lambda = 500$–520 nm) and on the angle of incidence (for $\theta_1 = 0°$–8°). Layer widths are fixed at $h_c = 7$ μm and $h_g = 150$ nm. Again we can see significant reflectance, within reflectance bands reaching a value 1, and quasiperiodical, resonancelike dependence on both λ and θ.

For the model there are simple formulas that link

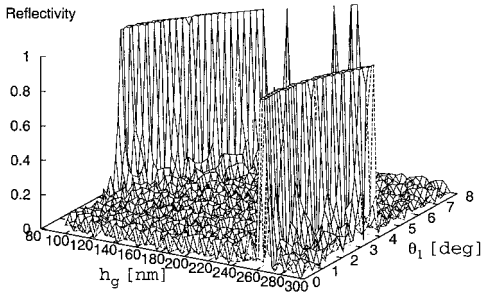

Fig. 6. Reflectivity $\mathcal{R}$ versus $\theta_1 = 0°$–8°; thickness of layers, $h_c = 7$ μm, $h_g = 100$–300 nm; $\lambda = 500$ nm.

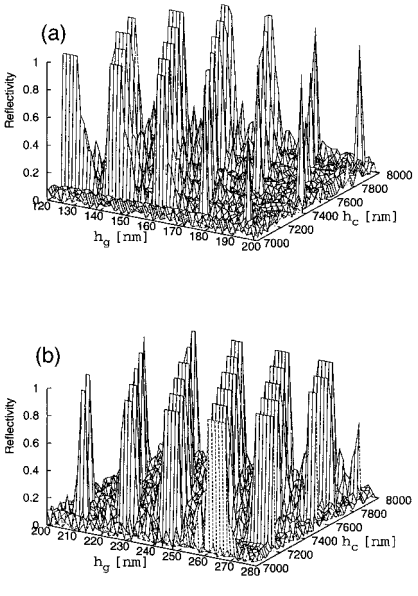

Fig. 8. Reflectivity $\mathcal{R}$ dependence versus thickness of layers: (a) $h_c = 7$–8 μm, $h_g = 120$–200 nm; (b) $h_g = 200$–280 nm, with $\theta_1 = 0°$, $\lambda = 500$ nm. The space pattern has two periods along the h_g axis (short and long).

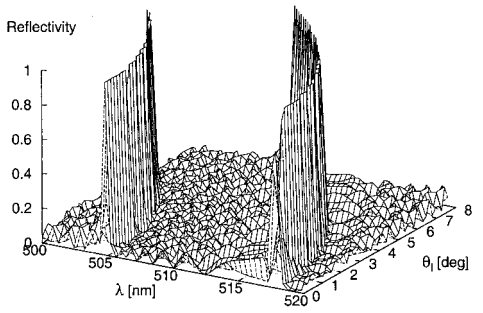

Fig. 9. Reflectivity $\mathcal{R}$ dependence versus angle of incidence $\theta_1 = 0°–8°$ and wavelength $\lambda = 500–520$ nm; $h_c = 7$ μm, $h_g = 150$ nm.

the azimuthal angle of the incident linearly polarized light with azimuthal angles of the reflected and transmitted light.[10] If $A_{\parallel}, A_{\perp}$ denote the amplitudes of parallel and transversal components of incident light, respectively, and azimuthal angle α_i is defined by

$$\tan \alpha_i = \frac{A_{\parallel}}{A_{\perp}}, \tag{35}$$

then it follows from Fresnel formulas that the azimuthal angles for the transmitted ray α_t and reflected ray α_r would be

$$\tan \alpha_r = \frac{\cos(\theta_i - \theta_t)}{\cos(\theta_i + \theta_t)} \tan \alpha_i, \tag{36}$$

$$\tan \alpha_t = \cos(\theta_i - \theta_t) \tan \alpha_i, \tag{37}$$

where θ_i, θ_t are the angles of incident and transmitted light, respectively (θ_t relates to θ_{i+1} in Fig. 3 for the last membrane in the pile). The light scattering of a normal lens is due to density fluctuations because only the $I_{\parallel}$ component of the polarized light yields a diffraction pattern and the $I_{\perp}$ component is absent.[5,17]

B. Equivalent Refractive Index and Thickness

It can be shown that such periodically stratified optical media are equivalent for a given wavelength, to a double-layer homogeneous component combination, with parallel boundaries and effective optical thickness β. Moreover, when the stratified medium is symmetrical {i.e., $n[1/2(z_j + z_{j+1}) + x] = n[1/2(z_j + z_{j+1}) - x]; x \le 1/2(z_{j+1} - z_j), j = 1, 2, \ldots, N$}, it was shown by Herpin[22] that such a symmetrical multilayer compound is equivalent to a single layer with equivalent refractive index and equivalent thickness, which may be different from all known material and will in general vary with wavelength. In fact, both equivalent refractive index and thickness may turn out to be complex even if the multilayer is nonabsorbing. In terms of elements of matrix $\mathcal{M}$ [see Eq. (30)], the equivalent optical thickness β_e and refractive index n_e are defined by[24]

$$\cos \beta_e = \mathcal{M}_{11} = \mathcal{M}_{22}, \tag{38}$$

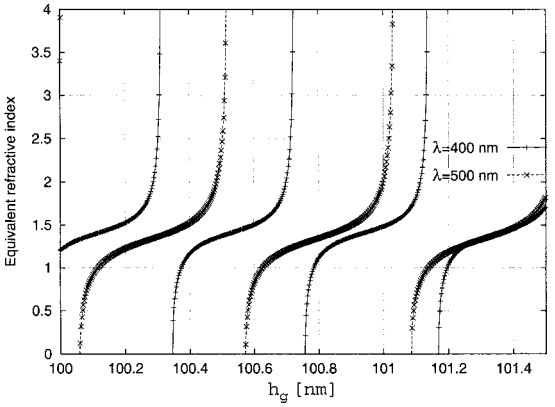

Fig. 10. Equivalent refractive index of the pile dependence versus thickness of gaps $h_g = 100–101.5$ nm. $h_c = 7$ μm and wavelength $\lambda = 400$ and 500 nm.

$$n_e = \frac{i \sin \beta_e}{\mathcal{M}_{12}} = \frac{-i\mathcal{M}_{21}}{\sin \beta_e}. \tag{39}$$

Figure 10 shows the dependence of the equivalent refractive index of the pile on the width of the gaps $h_g = 100–101.5$ nm and wavelength $\lambda = 400$ and 500 nm. The cell fiber thickness is assumed to be $h_c = 7$ μm. Only real values of n_e are plotted. The equivalent refractive index of the pile possesses strong nonlinear dependence on the gap width and can vary rapidly over wide ranges in a different way from real refractive indices of the layers.

It should be noted that the wavelength range of variance in Figs. 4–9 (500–520 nm) is nonspecific and was chosen in the midrange of the visible spectrum purely as an example. Figure 10 shows the wavelength dependence of the equivalent refractive index and shows that, as λ increases from 400 to 500 nm, the period λ_s of the stop zones increases also (≈1.25 times). At the same time, the equivalent refractive-index gradient and hence the reflectance become less steeply varying. When λ tends to infinity, the stop zones become less frequent and narrow (with the same maximum amplitude 1) and tend to vanish.

C. Discussion

It seems that the process of intraocular scattering as a whole is complex and multifactorial. Different factors will operate in different ways. The resonance mechanism described here does not contradict or reject existing known models of cataract turbidity.[1,2,30,31] Indeed, because none of the previous models discuss the proposed resonance, interference mechanism of scattering, our model serves to complement previous ones. It indicates that, in addition to known reasons for turbidity, multiple resonance reflectance could be another factor responsible for the light scatter and diffusion seen with cataract. This factor does not make the largest contribution to the amount of scattered light, but operates in conjunction with the other factors. As a consequence, the strong angular dependence of light scatter that this model

predicts does not predominantly characterize the process of the lenticular scattering.

It is worth noting that the resonance mechanism is peculiar to more or less regular structures. Such structures start to break down in the course of cataractogenesis. Indeed, in later stages of nuclear cataract in which cell membranes have undergone substantial degenerative changes, the structure of the lens tissue represents a highly disorganized chaotic media.[32] Obviously, the resonance effects discussed will not operate under such conditions. This also applies to cataracts in which the fluid-filled gaps between the cells are not well pronounced.

Any model dealing with structural influences on light transmission through the lens needs to make some assumptions and simplifications. Clearly the forward scatter and backscatter that are due to randomly distributed values of the layer thickness have a random fluctuation pattern. Our model has replaced the naturally occurring irregularities between the hexagonal fiber cell boundaries with a simple regular stratification. The natural irregularities would produce a greater anisotropy in refractive index, further enhancing reflectivity. However, our model shows that even a single incident beam results in a combination of reflected and transmitted beams, and this indicates that multiple reflections will occur in the eye lens because of its stratified morphology. These have a significant impact on light transmission and cannot be ignored in the modeling of scattering processes.

The effect of the narrow stop zones cannot be accurately predicted. The irregularity of the lens stratification may cause the light in the stop zones to undergo multiple reflections between the layers of the lens, culminating in diffusion and negligible light reaching the retina. This could cause coloration of the whole retinal image or a colored halo. Such effects are observed in cases of cataract and have been attributed to the effects of absorption in the lens tissue. As yet there has been no experimental evidence of any peaks in the visible absorption spectra of the cataractous lens.[33] Hence the proposed mechanism of the interference scattering may provide an explanation for such pseudoabsorption.

4. Conclusion

We have estimated the characteristics of light reflection of real experimental data from the morphological structure of the eye lens, modeled as a stratified pile of layers with different refractive indices. It was shown that the eye lens can possess the property of an interference filter with reflectance up to 1 in the visible spectrum. The reflectance mainly depends on refractive indices and widths of the layers (cell fibers and fluid-filled gaps). The dependence of reflectance on wavelength and on the angle of incidence of light was also studied. All these parameters can vary through the lens and presumably have a randomly organized spatial nature.

In view of this, it necessary to conduct further experimental investigation of spatial distribution characteristics, specifically the width and refractive index of cell fibers and gaps between the cells to see how these change with swelling and volume regulation.[14,18]

This research is supported by UK Engineering and Physical Sciences Research Council grant GR/M62679.

References and Note

1. G. B. Benedek, "Theory of transparency of the eye," Appl. Opt. **10,** 459–473 (1971).
2. G. B. Benedek, "Cataract as a protein condensation disease: the Proctor lecture," Invest. Ophthalmol. Visual Sci. **38,** 1911–1921 (1997).
3. B. K. Pierscionek and N. Y. C. Chan, "The refractive index gradient of the human lens," Invest. Ophthalmol. Visual Sci. **66,** 822–829 (1989).
4. B. K. Pierscionek, "Variation in refractive index and absorbance of 670 nm light with eye in cataract formation in human lens," Exp. Eye Res. **60,** 407–413 (1995).
5. F. A. Bettelheim and L. Siew, "Biological-physical basis of lens transparency," in *Cell Biology of the Eye*, D. S. McDevitt, ed. (Academic, New York, 1982).
6. J. M. Hogan, J. A. Alvarado, and J. E. Weddell, *Histology of the Human Eye* (Saunders, Philadelphia, Pa., 1971).
7. R. P. Hemenger, "Small-angle intraocular light scatter: a hypothesis concerning its source," J. Opt. Soc. Am. A **5,** 577–582 (1988).
8. R. Jacobsson, "Light reflection from films of continuously varying refractive index," in *Progress in Optics*, E. Wolf, ed. (North-Holland, Amsterdam, 1965), Vol. 5, pp. 247–286.
9. L. Epstein, "The design of optical filters," J. Opt. Soc. Am. **42,** 806–810 (1952).
10. H. A. Macleod, *Thin-Film Optical Filters* (Hilger, London, 1969).
11. M. Born and E. Wolf, eds., *Principles of Optics* (Pergamon, New York, 1970).
12. F. A. Bettelheim and S. Ali, "Light scattering of normal human lens. III. Relationship between forward and back scatter of whole excised lenses," Exp. Eye Res. **41,** 1–9 (1985).
13. B. A. Moffat, K. A. Landman, R. J. Trascott, M. H. Sweeney, and J. M. Pope, "Age-related changes in the kinetics of water transport in normal human lenses," Exp. Eye Res. **69,** 663–669 (1999).
14. T. J. Jacob, "The relationship between cataract, cell swelling and volume regulation," Prog. Retinal Eye Res. **12,** 223–233 (1999).
15. R. Courant and D. Hilbert, *Methoden der Mathematischen Physic* (Springer-Verlag, Berlin, 1993).
16. W. Driscoll, ed., *Handbook of Optics* (McGraw-Hill, New York, 1978).
17. F. A. Bettelheim and M. Paunovic, "Light scattering of normal human lens," Biophys. J. **26,** 85–100 (1973).
18. F. A. Bettelheim, A. C. Churchill, and J. S. Zigler, "On the nature of hereditary cataract in strain 13/N guinea pigs," Curr. Eye Res. **16,** 917–924 (1997).
19. P. G. Bracchi, F. Carta, P. Fasella, and G. Maraimi, "Selective binding of age α-crystallin to lens fiber ghost," Exp. Eye Res. **12,** 151–154 (1971).
20. A. P. Beers, G. L. van der Heijde, and M. Dubbelman, "Aging of crystalline lens and presbyopia," Tijdschr. Gerontol. Geriatr. **29,** 185–188 (1998).
21. F. Abelès, "Recherches sur la propagation des ondes électromagnétiques sinusoidales dans les milieux stratifiés. Application aux couches minges," Ann. Phys. (Paris) **5,** 596–640, 706–782 (1950).

22. A. Herpin, “Calcul du pouvoir réflecteur d’un systéme stratifié quelconque,” C. R. Sceances Acad. Sci. **225,** 182–183 (1947).
23. C. Dufour and A. Herpin, “Propogation des ondes électromagnétiques dans un milieu stratifié périodique transparent,” Rev. Opt. Theor. Instrum. **32,** 321–348 (1953).
24. W. Weinstein, “Computations in thin film optics,” Vacuum **4,** 3–19 (1954).
25. M. Abramovitz and I. Stegun, *Handbook of Mathematical Functions, with Formulas, Graphs and Mathematical Tables* (Dover, New York, 1965).
26. G. B. Benedek, J. I. Clark, E. N. Serrallach, C. Y. Young, L. Mengel, T. Sauke, A. Bagg, and K. Benedek, “Light scattering and reversible cataracts in the calf and human lens,” Philos. Trans. R. Soc. London Ser. A **293,** 329–340 (1979).
27. B. K. Pierscionek, “Refractive index contours in the human lens,” Exp. Eye Res. **64,** 887–893 (1997).
28. A. Thelen, “Multilayer filters with wide transmittance bands,” J. Opt. Soc. Am. **53,** 1266–1270 (1963).
29. A. Thelen, “Equivalent layers in multilayer filters,” J. Opt. Soc. Am. **56,** 1533–1538 (1966).
30. B. Pierscionek, R. Green, and S. G. Dolgobrodov are preparing a manuscript to be called “Calculation of retinal image for cataractous eye as modeled through a phase aberrating medium.”
31. J. L. Zuckerman, D. Miller, W. Dyes, and M. Keller, “Degradation of vision through a simulated cataract,” Invest. Ophthalmol. **12,** 213–224 (1973).
32. B. Philipson, “Changes in the lens related to the reduction of transparency,” Exp. Eye Res. **16,** 29–39 (1973).
33. B. Philipson, “Biophysical studies on normal and cataractous rat lenses,” Acta Ophthalmol. Suppl. **103,** 1–30 (1969).